

Multiband light curves of tidal disruption events

Giuseppe Lodato¹* and Elena M. Rossi²

¹*Dipartimento di Fisica, Università Degli Studi di Milano, Via Celoria, 16, Milano 20133, Italy*

²*Racah Institute of Physics, The Hebrew University, Jerusalem 91904, Israel*

Accepted 2010 July 28. Received 2010 July 20; in original form 2010 May 27

ABSTRACT

Unambiguous detection of the tidal disruption of a star would allow an assessment of the presence and masses of supermassive black holes in quiescent galaxies. It would also provide invaluable information on bulge-scale stellar processes (such as two-body relaxation) via the rate at which stars are injected into the tidal sphere of influence of the black holes. This rate, in turn, is essential to predict gravitational radiation emission by compact object inspirals. The *signature* of a tidal disruption event is thought to be a fallback rate for the stellar debris on to the black hole that decreases as $t^{-5/3}$. This mass flux is often assumed to yield a luminous signal that decreases in time at the same rate. In this paper, we calculate the monochromatic light curves arising from such an accretion event. Differently from previous studies, we adopt a more realistic description of the fallback rate and of the super-Eddington accretion physics. We also provide simultaneous light curves in optical, ultraviolet (UV) and X-rays. We show that, after a few months, optical and UV light curves scale as $t^{-5/12}$, and are thus substantially flatter than the $t^{-5/3}$ behaviour, which is a prerogative of the bolometric light curve, only. At earlier times and for black hole masses $< 10^7 M_{\odot}$, the wind emission dominates: after reaching a peak of $10^{41}–10^{43} \text{ erg s}^{-1}$ at roughly a month, the light curve decreases steeply as $\sim t^{-2.6}$, until the disc contribution takes over. The X-ray band, instead, is the best place to detect the $t^{-5/3}$ ‘smoking gun’ behaviour, although it is displayed only for roughly a year, before the emission steepens exponentially.

Key words: black hole physics – hydrodynamics – galaxies: nuclei.

1 INTRODUCTION

Luminous flares from quiescent (non-active) galaxies are often interpreted as arising from the tidal disruption of stars as they get close to a dormant supermassive black hole in the centre of the galaxy (Komossa & Bade 1999; Esquej et al. 2008; Gezari et al. 2008, 2009; Cappelluti et al. 2009). If this interpretation is correct, such events represent a very important probe for black holes in quiescent galaxies. In principle, detailed modelling of individual events could yield constraints on black hole properties. More ambitiously, a measurement of the rate of events in galaxies of different types would provide information on the stellar dynamics at parsec scales that is responsible for injecting stars into orbits that result in tidal disruption (e.g. Magorrian & Tremaine 1999; Syer & Ulmer 1999). Knowledge of these stellar dynamical processes is of broad interest, since similar processes contribute to the rate of at which compact objects are captured by (and subsequently merge with) the central black hole (Sigurdsson & Rees 1997). These extreme mass ratio inspirals are important targets for future gravitational wave experi-

ments. Similar processes also occur for lower mass objects, such as in compact binary systems, hosting (i) a stellar mass black hole and a white dwarf (Rosswog, Ramirez-Ruiz & Hix 2008); or (ii) two white dwarfs (Rosswog 2007; Rossi & Begelman 2009).

The pioneering works by Lacy, Townes & Hollenbach (1982), Rees (1988), Phinney (1989) and, from a numerical point of view, by Evans & Kochanek (1989) have set the theoretical standard for the interpretation of such events. In particular, a distinctive feature of this theory is that, to a first approximation, the rate at which the black hole is fed with the stellar debris after the tidal disruption (the ‘fallback rate’ \dot{M}_{fb}) should decrease as¹ $\dot{M}_{\text{fb}}(t) \propto t^{-5/3}$. If the fallback rate can be directly translated into an accretion luminosity, one could then expect the light curve of such events to follow the same behaviour with time. Indeed, a $t^{-5/3}$ light curve is generally fitted to the observed luminosities of events interpreted as stellar disruptions (Esquej et al. 2008; Gezari et al. 2008, 2009; Cappelluti et al. 2009). In practice, the $t^{-5/3}$ evolution of the fallback rate is valid only after several months from the event, and the initial evolution generally

*E-mail: giuseppe.lodato@unimi.it

¹Note that the original paper by Rees (1988) quotes a $t^{-5/2}$ dependence, later corrected to $t^{-5/3}$ by Phinney (1989).

shows a relatively gentle rise with time, dependent on the internal structure of the disrupted star (Lodato, King & Pringle 2009).

However, it is not obvious *a priori* that one can make such a direct translation of the fallback rate into observed luminosity, for a number of reasons. First, for small black hole masses and at optical frequencies, Strubbe & Quataert (2009) showed that the emission can contain at early times a significant component arising from a radiatively driven wind, consequence of an initial super-Eddington fallback rate. Additionally, the unbound stellar debris might also give some contribution at optical wavelengths (Kasen & Ramirez-Ruiz 2010). Secondly, observations are typically made in some narrow bands. Since the system is intrinsically time variable, this implies that the monochromatic light curves should not necessarily scale at all times with the bolometric curve.

In this paper, we consider systematically both effects and we show that, in general, the expected monochromatic light curve in most bands does not scale as $t^{-5/3}$. When the luminosity is dominated by the accretion of the fallback material, at optical and UV frequencies, the light curve is proportional to $t^{-5/12}$ during an extended period of time. Only in X-rays one should expect a light curve close to the naive expectation and only for a brief period of time. Additionally, during the first year or so since disruption, the wind emission may further complicate the shape of the light curve in the optical and in the UV bands. We show that the strength of this contribution depends on the internal structure of the disrupted star and on the fraction of mass that the black hole can accrete, when fed at a super-Eddington rate.

This paper is organized as follows. In Section 2, we review the basic dynamics involved in a tidal disruption event. In Section 3, we demonstrate analytically what are the expected monochromatic light curves of the disc and of the wind emission, separately. In Section 4, we discuss the full light curve in several bands, as a function of the main parameters of our model. In Section 5, we discuss our results and draw our conclusions.

2 BASIC DYNAMICS

Let us consider a star with mass $M_* = m_* M_\odot$ and radius $R_* = x_* R_\odot$, which moves in a highly eccentric orbit under the sole influence of a supermassive black hole with mass $M = 10^6 M_6 M_\odot$. If the distance of closest approach, r_p , to the black hole is within the tidal sphere of radius

$$r_t = \left(\frac{M}{M_*}\right)^{1/3} R_* \approx 0.47 \text{ au} \left(\frac{M_6}{m_*}\right)^{1/3} x_*, \quad (1)$$

then the star self-gravity is not able to counteract the tidal pull and the star is torn apart. We define the penetration factor as the ratio of the two distances:

$$\beta \equiv \frac{r_t}{r_p}. \quad (2)$$

When needed, our standard choice of parameters for the stellar properties is $\beta = x_* = m_* = 1$.

For simplicity, we will assume the star trajectory to be parabolic. However, the dynamics described here is more generally valid for stars whose orbital energy is much smaller than the energy spread caused by tidal forces. The stars that enter the tidal sphere are generally expected to satisfy this requirement, since they should have very eccentric orbits.

At distances r larger than r_t , $R_*/r \leq (M_*/M)^{1/3} \approx 10^{-2}$ and the star behaves effectively as a point mass in the black hole gravitational field. However, when the star approaches its pericentre

$r_p \approx r_t$, the star size becomes important. The different distances to the black hole at which different fluid elements lie cause a sizeable spread $\Delta\epsilon$ in specific energy ϵ within the star:

$$\Delta\epsilon \simeq \pm \frac{GM}{r_p^2} R_* \quad (3)$$

(Lodato et al. 2009), which can greatly exceed the star-binding energy $\Delta\epsilon/(GM_*/R_*) = \beta^2 (M/M_*)^{1/3}$. As a result of this spreading, half of the star debris remains bound ($\epsilon < 0$) to the black hole, while the rest ($\epsilon > 0$) is lost from the system.² The material, which remains bound, lies in highly eccentric orbits and after a time

$$\begin{aligned} t_{\min} &= \frac{2\pi GM}{(-2\Delta\epsilon)^{3/2}} \\ &= \frac{\pi}{2^{1/2}} \left(\frac{r_p}{R_*}\right)^{3/2} \sqrt{\frac{r_p^3}{GM}} \\ &\approx 41 M_6^{1/2} m_*^{-1} \beta^{-3} x_*^{3/2} \text{ d}, \end{aligned} \quad (4)$$

it starts coming back to pericentre at a rate \dot{M}_{fb} , which depends on the distribution of specific energies. If the distribution in energy $dM_*/d\epsilon$ is flat, then we find the classic result (Rees 1988; Phinney 1989):

$$\dot{M}_{\text{fb}} = \dot{M}_p \left(\frac{t}{t_{\min}}\right)^{-5/3}. \quad (5)$$

The peak fallback rate

$$\dot{M}_p = \frac{1}{3} \frac{M_*}{t_{\min}} \approx 1.9 \times 10^{26} M_6^{-1/2} m_*^2 \beta^3 x_*^{-3/2} \text{ g s}^{-1} \quad (6)$$

can be compared to the Eddington accretion rate

$$\dot{M}_{\text{Edd}} = 1.3 \times 10^{24} M_6 \left(\frac{\eta}{0.1}\right)^{-1} \text{ g s}^{-1} \quad (7)$$

where $\eta \approx 0.1$ is the radiative efficiency of the accretion process. We thus see that for a $10^6 M_\odot$ black hole, the fallback rate can be as large as 100 times the Eddington rate, and is therefore expected to produce a luminous flare, which can be, in principle, detectable. Note that the ratio $\dot{M}_p/\dot{M}_{\text{Edd}} \propto M^{-3/2}$, so that the fallback rate is expected to be only marginally super-Eddington for a $10^7 M_\odot$ black hole. Although also in this case a luminous flare is expected to be produced, its appearance will be significantly different, as discussed below in Section 4. After a time

$$t_{\text{Edd}} = 760 \left(\frac{\eta}{0.1}\right)^{3/5} M_6^{-2/5} m_*^{1/5} \beta^{-6/5} x_*^{3/5} \text{ d}, \quad (8)$$

the fallback rate ceases to be super-Eddington.

This simple picture has been extensively tested numerically (Nolthenius & Katz 1982; Evans & Kochanek 1989; Laguna et al. 1993; Ayal, Livio & Piran 2000). In particular, Lodato et al. (2009) showed two important results that we will use in the following. First, even when $\beta = 1$ and the spin-up of the star is expected to approach the break-up velocity, equation (3) is a good estimate for the total energy spread. Secondly, the energy distribution $dM_*/d\epsilon$ within the bound matter depends on the internal structure of the star (parametrized by its polytropic index γ). In particular, they found that $dM_*/d\epsilon$ is constant only for an idealized incompressible star ($\gamma \gg 1$). In this idealized case, \dot{M}_{fb} follows equation (5) at all times. In general, however, the resulting \dot{M}_{fb} departs from the $t^{-5/3}$ power-law behaviour, during the first few months (see their

² If the stellar orbit is not exactly parabolic, then the ratio of bound versus unbound material may vary.

fig. 10, left-hand panel), resulting in a smaller peak fallback rate. The departure is more pronounced for more compressible stellar models.

As matter falls back to r_p , we assume that it undergoes shocks that convert part of its kinetic energy into internal energy. Initially, when the accretion rate is highly super-Eddington, only a fraction $(1 - f_{\text{out}})$ of the fallback material forms a disc and can accrete all the way down to the black hole. The remaining part of the stellar debris will instead leave the system under a strong radiative pressure. It is not possible to quantify analytically the parameter f_{out} , because the amount of mass that is ejected will depend upon the detailed redistribution of energy and angular momentum within the flow (Blandford & Begelman 2004). Rather, simulations are required to assess the rate at which a hole can be fed in such extreme conditions. Strubbe & Quataert (2009) assumed a constant $f_{\text{out}} = 0.1$. For moderate super-Eddington accretion rates, however, numerical slim disc models by Dotan & Shaviv (2010) indicate that f_{out} is a growing function of $\dot{M}_{\text{fb}}/\dot{M}_{\text{Edd}}$, reaching $f_{\text{out}} \approx 0.7$ for $\dot{M}_{\text{fb}}/\dot{M}_{\text{Edd}} = 20$. For higher accretion rates, they could not find steady-state solutions. This does not mean that solutions with a different accretion geometry do not exist. However, it does mean that any extrapolation of their results to more vigorous accretion regimes, that may be attained as a consequence of a tidal disruption event, should be considered as indicative. Mindful of these uncertainties, we will explore the consequences of different prescriptions for f_{out} .

The material, which is not ejected in the wind, accretes on to the black hole through a relatively thick disc. Initially, the disc viscous time is much shorter than the time-scale at which the material falls back to r_p . In this phase, the rate at which the black hole accretes mass is thus the same as the rate at which the disc is fed from the fallback material. At very late times (at $t \gtrsim 100$ yr after the event, e.g. Ulmer 1999), the viscous time becomes long enough that the accretion rate is controlled by viscous processes rather than by the disc feeding. Cannizzo, Lee & Goodman (1990) have discussed these late stages and found that the accretion rate on to the hole scales as $t^{-1.2}$. In this paper, we will not consider these late stages, focussing instead on the early evolution of the system.

3 SCALINGS FOR THE MULTIWAVELENGTH EMISSION

In this section, we discuss the relevant dynamics and radiative properties of the disc and the wind separately. In particular, we will focus on the temporal behaviour of monochromatic light curves, which are derived analytically assuming a pure $t^{-5/3}$ power law for the accretion rate. Therefore, these scalings should be regarded as being only suggestive at early times (<half a year). However, they certainly provide a good description at times larger than 1 yr after disruption, when the observed emission is dominated by the disc at all frequencies (see Section 4).

3.1 Disc contribution

In this section, we focus on the disc emission, which is expected to dominate at high frequencies and/or at late times. For simplicity, we adopt here a thin disc geometry and defer to Section 4 a discussion of a probably more realistic slim disc model. For a geometrically thin and optically thick disc, the effective temperature at a given radius R is related to the mass accretion rate through

$$\sigma_{\text{SB}} T_{\text{d}}^4 = \frac{3GM\dot{M}}{8\pi R^3} \left(1 - \sqrt{\frac{R_{\text{in}}}{R}}\right), \quad (9)$$

where M is the black hole mass, $\dot{M} = (1 - f_{\text{out}})\dot{M}_{\text{fb}}$ is the accretion rate, $R_{\text{in}} \approx 3R_{\text{S}}$ (where $R_{\text{S}} = 2GM/c^2$ is the Schwarzschild radius of the black hole) and σ_{SB} is the Stefan–Boltzmann constant. As time increases, the accretion rate decreases as $t^{-5/3}$. Thus, while the bolometric luminosity scales as \dot{M} , the disc temperature decreases as $\dot{M}^{1/4}$.

For a star of mass $M_{\star} = M_{\odot}$ and radius $R_{\star} = R_{\odot}$, disrupted by a $10^6 M_{\odot}$ black hole, the tidal radius is approximately at $20R_{\text{S}}$ from the hole (equation 1). Since the disc outer radius is expected to be close to the circularization radius $R_{\text{out}} = 2r_p = 2r_t/\beta$, the radial extent of the disc is rather small. In general, we have

$$\frac{R_{\text{out}}}{R_{\text{in}}} \simeq 15 \beta^{-1} M_6^{-1/2} m_{\star}^{-1/3} x_{\star}, \quad (10)$$

The spectrum of an optically thick disc is approximately given by a superposition of blackbody spectra with temperature ranging from $T_{\text{out}} = T(R_{\text{out}})$ to $T_{\text{in}} = T(R_{\text{in}})$. Since the radial extent of the disc is small, the range of disc temperatures is correspondingly small

$$\frac{T_{\text{in}}}{T_{\text{out}}} \simeq \left(\frac{R_{\text{out}}}{R_{\text{in}}}\right)^{3/4} \approx 7.6 \beta^{-3/4} M_6^{-3/8} m_{\star}^{-1/4} x_{\star}^{3/4}. \quad (11)$$

If the event is observed at a given wavelength ν_{obs} , we may define a corresponding temperature through Wien's displacement law

$$T_{\text{obs}} \approx 1.7 \times 10^4 \nu_{15} \text{ K}, \quad (12)$$

where we adopt the notation: $\nu_x = \nu_{\text{obs}}/10^x$ Hz. The shape of the light curve is determined by the relative size of T_{obs} , T_{in} and T_{out} . We can identify three phases:

(a) $T_{\text{obs}} < T_{\text{out}}$: This corresponds to the earliest times (when the disc is hotter) for relatively small observed frequencies. In this case, the observed frequency sits in the Rayleigh–Jeans tail of the disc spectrum and thus the luminosity scales with time in the following way:

$$\nu L_{\nu} \propto T_{\text{d}} \propto \dot{M}^{1/4} \propto t^{-5/12}. \quad (13)$$

(b) $T_{\text{out}} < T_{\text{obs}} < T_{\text{in}}$: In this phase, the emission at ν_{obs} is dominated by the disc radii for which $T(R) \approx T_{\text{obs}}$, whose flux is close to the bolometric flux. Since the emitting area does not vary much with time (at most by a factor $R_{\text{out}}/R_{\text{in}} \approx 10$), it is in this phase that we can expect a monochromatic luminosity proportional to $t^{-5/3}$.

(c) $T_{\text{in}} < T_{\text{obs}}$: This phase occurs at late times, when the disc has cooled significantly. In this case, the observed frequency sits in the Wien part of the spectrum and we should expect an exponentially declining monochromatic light curve.

The transition between the different phases occurs at times t_{ab} and t_{bc} , such that $T_{\text{out}}(t_{\text{ab}}) = T_{\text{obs}}$ and $T_{\text{in}}(t_{\text{bc}}) = T_{\text{obs}}$. These two transition times are given by

$$t_{\text{ab}} \approx 6.3 \times 10^4 \beta^{3/5} M_6^{1/5} m_{\star}^{4/5} x_{\star}^{-6/5} \nu_{15}^{-12/5} \text{ d}, \quad (14)$$

$$t_{\text{bc}} \approx 8.4 \times 10^6 \beta^{-6/5} M_6^{-1} m_{\star}^{1/5} x_{\star}^{3/5} \nu_{15}^{-12/5} \text{ d}. \quad (15)$$

Typically, these transitions occur at times much larger than t_{Edd} , and we have thus assumed $f_{\text{out}} = 0$ in equations (14) and (15). We plot in Fig. 1 the relevant time-scales as a function of the black hole mass M_6 for three choices of the observed frequency: $\nu_{\text{obs}} = 6.3 \times 10^{14}$ Hz (optical g band), $\nu_{\text{obs}} = 1.9 \times 10^{15}$ Hz (the GALEX FUV band) and $\nu_{\text{obs}} = 4.8 \times 10^{16}$ Hz (soft X-rays at 0.2 keV). The solid line shows the time t_{min} , which marks the beginning of the tidal disruption event. The short-dashed line indicates t_{ab} and the long-dashed line indicates t_{bc} . We thus clearly see that in the optical and in the FUV, the light curve initially follows a $t^{-5/12}$ light curve for an

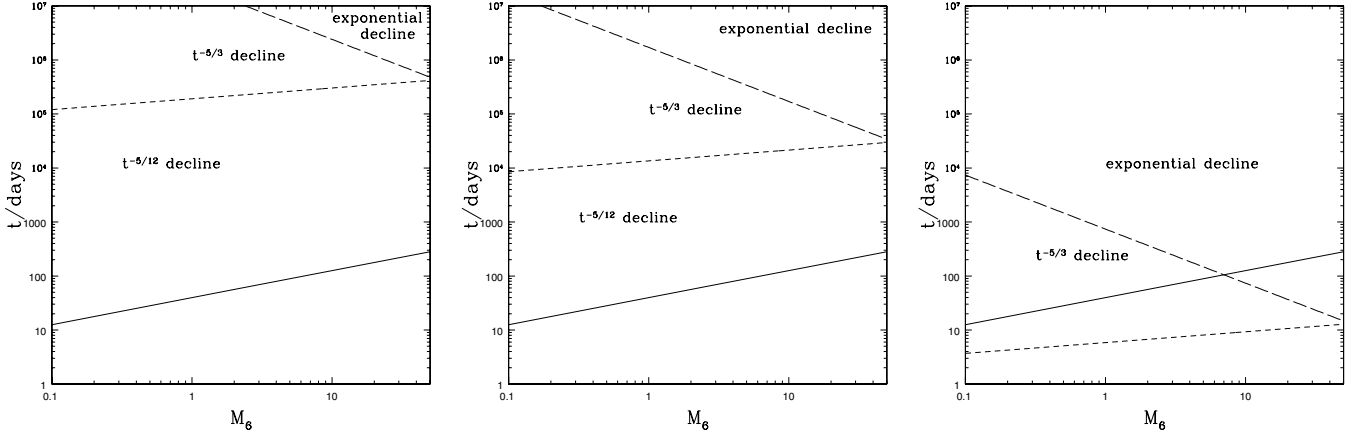


Figure 1. Typical time-scales as a function of the black hole mass. The solid line shows t_{\min} (equation 4), the short-dashed line shows t_{ab} and the long-dashed line shows t_{bc} . The three panels refer to an observed frequency in the optical g band (left-hand panel), in the GALEX FUV band (middle panel) and in the X-rays at 0.2 keV (right-hand panel). In the optical and FUV, for an extended period of time after the event, the light curve is expected to scale as $t^{-5/12}$ before steepening into $t^{-5/3}$. It is only in X-rays that the initial light curve follows the standard $t^{-5/3}$ law.

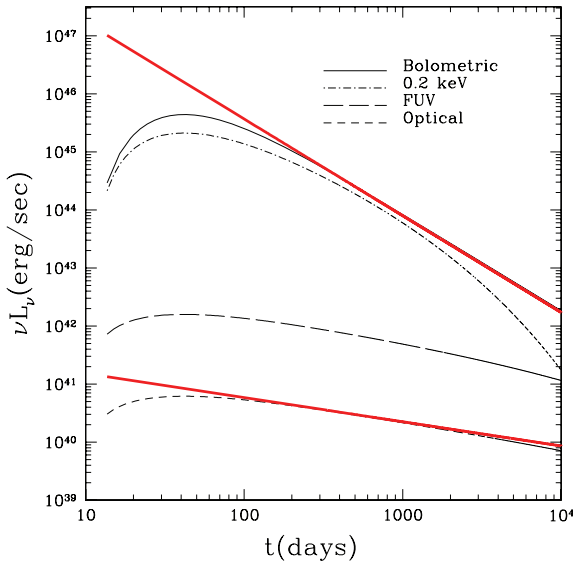


Figure 2. Light curves for the disc emission from the disruption of a solar-type star by a $10^6 M_{\odot}$ black hole at $\beta = 1$. The fallback rate corresponds to a $\gamma = 1.4$ polytropic model for the star (Lodato et al. 2009). The time $t = 0$ corresponds to the pericentre passage of the disrupted star. The solid line shows the bolometric luminosity, the dot-dashed line shows the luminosity at 0.2 keV, the long-dashed line shows the luminosity in the FUV, at $\nu = 1.9 \times 10^{15}$ Hz, while the short-dashed line shows the luminosity in the optical at $\nu = 6.3 \times 10^{14}$ Hz. The two red lines mark the simple power laws expected for the bolometric luminosity ($\propto t^{-5/3}$) and for the monochromatic luminosity in the optical/UV ($\propto t^{-5/12}$).

extended period of time, lasting several hundred years for the g band and several decades for the GALEX FUV band. Only in the X-rays is the initial light curve expected to show the standard $t^{-5/3}$ decline for a few years, before turning into an exponential decline. Note also that the time-span during which we expect a monochromatic $t^{-5/3}$ decline gets smaller for higher black hole masses, at all frequencies.

An example of a disc light curve at different frequencies is shown in Fig. 2, which corresponds to a solar type star disrupted by a $10^6 M_{\odot}$ black hole. The fallback rate is the one predicted by Lodato et al. (2009) for a $\gamma = 1.4$ polytropic model for the star. The two red lines trace, for comparison, a $t^{-5/3}$ and a $t^{-5/12}$ decline. This

figure confirms the simple estimates described above: the optical and FUV light curves show, initially, a $t^{-5/12}$ decline, while the X-ray light curve follows the bolometric $t^{-5/3}$ curve; after a few years, the X-ray light curve steepens into an exponential decline.

3.2 Wind contribution

In this section, we derive the monochromatic luminosity scalings for the wind contribution to the emission that may arise from a tidally disrupted star.

The main properties of a radiation-driven wind powered by fallback matter have been calculated by Rossi & Begelman (2009) and applied to the problem at hand by Strubbe & Quataert (2009). Here, we state some of their main results without derivation and we refer the reader to that literature for more details. In addition, we derive scalings to better illustrate the behaviour of a monochromatic light curve.

The main assumptions are the following. From the launching radius $r_{\text{L}} \approx R_{\text{out}}$, the wind expands adiabatically and radially, with a constant velocity v_{w} , which we parametrize as a factor $f_{\text{v}} \geq 1$ times the escape velocity $\sqrt{2GM}/r_{\text{L}}$,

$$v_{\text{w}} \approx 4.4 \times 10^9 f_{\text{v}} \beta^{1/2} M_6^{1/3} x_{\star}^{-1/2} m_{\star}^{1/6} \text{ cm s}^{-1}. \quad (16)$$

This is justifiable, because R_{out} is close to the sonic radius, after which the velocity varies only by a factor of a few. We note that the two wind parameters, f_{v} and f_{out} , should be determined and related by global conservation of energy and mass for the whole system. However, given the level of simplification of our model, we do not attempt to calculate this relationship, which depends on the details of how energy and mass are actually redistributed between the disc and the wind. For this reason, in the following, we will treat these parameters as independent.

The radiation is advected with the flow up to the trapping radius, where the optical depth is $\tau \simeq c/v_{\text{w}}$. Afterwards, the radiative transfer takes over, until photons reach the photospheric radius r_{ph} . Since $c/v_{\text{w}} \approx 7$, the trapping radius and the photosphere are close enough that we may assume that the radiation keeps cooling along the same adiabatic curve for the whole evolution. As we show in the following, the temperatures in the flow are high enough to justify the use of a constant Thomson opacity for a fully ionized gas $\kappa_{\text{s}} = 0.4 \text{ g cm}^{-2}$.

The radiation temperature at the base of the wind, $T_L \equiv T(r_L)$, can be derived from energy conservation in the wind. If all the internal energy at the base of the wind is converted into kinetic energy at large distances, then the conservation law can be written as

$$4\pi r_L^2 v_w \left(\frac{4}{3} a T_L^4 \right) \simeq \frac{1}{2} \dot{M}_{\text{fb}} f_{\text{out}} v_w^2, \quad (17)$$

from which we get

$$T_L(t_{\text{min}}) \approx 3.5 \times 10^5 (f_{\text{out}} f_v)^{1/4} \beta^{11/8} M_6^{-5/24} x_*^{-1} m_*^{17/24} \text{ K}. \quad (18)$$

However, the wind is highly opaque and photons are released only at a much larger radius, the photospheric radius

$$r_{\text{ph}}(t_{\text{min}}) \approx 1.4 \times 10^{15} \left(\frac{f_{\text{out}}}{f_v} \right) \beta^{5/2} M_6^{-5/6} x_*^{-1} m_*^{11/6} \text{ cm}, \quad (19)$$

which is ~ 100 times r_L . The corresponding photospheric temperature $T_{\text{ph}} = T_L(r_{\text{ph}}/r_L)^{-2/3} (f_{\text{out}}/f_v)^{1/3}$, given by

$$T_{\text{ph}}(t_{\text{min}}) \approx \frac{1.6 \times 10^4}{\beta^{23/24}} x_*^{1/3} \left(\frac{f_v}{f_{\text{out}}} \right)^{1/12} \left(\frac{M_6^{41}}{m_*^{53}} \right)^{1/72} \text{ K}. \quad (20)$$

This gives an initial flash, most luminous in the optical band. As the accretion rate decreases, the photosphere sinks inwards as

$$r_{\text{ph}} = r_{\text{ph}}(t_{\text{min}}) \left(\frac{t}{t_{\text{min}}} \right)^{-5/3}, \quad (21)$$

and the corresponding temperature *increases* in time as

$$T_{\text{ph}} = T_{\text{ph}}(t_{\text{min}}) \left(\frac{t}{t_{\text{min}}} \right)^{25/36}. \quad (22)$$

If initially (at t_{min}) the observed frequency ν_{obs} lies much *below* the blackbody peak frequency, then the monochromatic light curve decreases quite steeply as

$$\nu_{\text{obs}} L_\nu \propto r_{\text{ph}}^2 T_{\text{ph}} \propto t^{-95/36}. \quad (23)$$

The peak in the light curve is thus at $t = t_{\text{min}}$,

$$\begin{aligned} \nu_{\text{obs}} L_\nu |_{t_{\text{min}}} &= \frac{8\pi^2 \nu_{\text{obs}}^3}{c^2} k T_{\text{ph}}(t_{\text{min}}) r_{\text{ph}}(t_{\text{min}})^2 \\ &\approx 3.7 \times 10^{41} \nu_{14}^3 \beta^{97/24} \left(\frac{f_{\text{out}}^{23}}{f_v^{17}} \right)^{1/12} \left(\frac{m_*^{211}}{M_6^{79}} \right)^{72} x_*^{-5/3} \text{ erg s}^{-1}, \end{aligned} \quad (24)$$

which, in the optical band, can be 10^{-2} – 10^{-3} of the Eddington luminosity.

When, instead, the observed frequency initially lies in the Wien part of the spectrum, then the light curve has an initial exponential rise. The time of the peak is reached when T_{ph} (equation 22) equals T_{obs} (equation 12):

$$t_{\text{max}} \approx 1.2 \times 10^3 \left(\frac{\nu_{16}^{36}}{M_6^8} \right)^{1/25} \left(\frac{f_{\text{out}}^3}{f_v^{21}} \right)^{1/25} \left(\frac{m_*^3 x_*^{51}}{\beta^{81}} \right)^{1/50} \text{ d}. \quad (25)$$

Afterwards, the light curve decreases as equation (23). The peak luminosity in this case is

$$\begin{aligned} \nu_{\text{obs}} L_{\nu, v} |_{t_{\text{max}}} &= 4\pi r_{\text{ph}}(t_{\text{max}})^2 \sigma T_{\text{obs}}^4 \\ &= 1.5 \times 10^{43} \nu_{16}^{-4/5} m_*^{2/15} \left(\frac{\beta}{x_*} \right)^{2/5} \left(\frac{f_{\text{out}}^8}{f_v^{24}} \right)^{1/5} M_6^{16/15} \text{ erg s}^{-1}. \end{aligned} \quad (26)$$

If the observed frequency is in X-rays, at 0.2 keV, the peak emission is $\approx 10^{41}$ erg s $^{-1}$ at $t_{\text{max}} \approx 9000$ d (for $f_{\text{out}} = 0.1$), which means that the wind contribution in the X-ray is much lower than the disc one (see Fig. 2) for the whole duration of the wind $t \leq t_{\text{edd}}$. Note that for the example above, $t_{\text{max}} \approx 9000$ d $\gg t_{\text{edd}}$, so the peak in

the soft X-ray light curve is never reached, because the wind ceases before.

In reality, the fallback rate may not be a pure power law, but rather an exponentially increasing function, followed by a plateau, which will then lead to the $t^{-5/3}$ decreasing slope. This has three main consequences. First, the duration of the super-Eddington phase (thus of the wind) may be shorter. Then, lower accretion rates are attained with respect to the power-law extrapolation at early times. Finally, there may be two spectral breaks in the light curve, since at early times, when \dot{M} increases, the photospheric temperature *decreases*, while at late times, when \dot{M} decreases, the opposite occurs. Therefore, it may be possible that the peak of the blackbody spectrum crosses twice the observed frequency.

4 TOTAL LIGHT CURVE

Having discussed the fundamental scalings of the two components of the emission separately, we now turn our attention to the total light curve. In particular, we discuss the consequences of relaxing two of our previous main assumptions: (i) that the fallback rate follows a simple power-law decline at all times; and (ii) that the gas fraction ejected through a radiative wind f_{out} is constant, independent of the fallback rate. Also, we will adopt a slim disc configuration during the super-Eddington phase, where the characteristic disc temperature is modified as

$$\sigma_{\text{SB}} T_{\text{d}}^4 = \frac{3GM\dot{M}f}{8\pi R^3} \left\{ \frac{1}{2} + \left[\frac{1}{4} + \left(\frac{\dot{M}}{\eta \dot{M}_{\text{Edd}}} \right)^2 \left(\frac{R_{\text{s}}}{R} \right)^2 \right] \right\}^{-1} \quad (27)$$

(Strubbe & Quataert 2009), where $f = 1 - \sqrt{R_{\text{in}}/R}$. The accretion rate in the disc is given by $\dot{M} = (1 - f_{\text{out}})\dot{M}_{\text{fb}}$, where the fallback rate is computed either from the analytical expression (equation 5) or from the numerical results of Lodato et al. (2009), depending on the models. From equation (27), we directly compute the disc effective temperature, which allows us to compute the monochromatic luminosities as a function of time.

4.1 Modelling the fallback rate: wind suppression

As mentioned above, equations (5) and (6) only hold under the assumption that the specific energy distribution within the disrupted star is constant. As shown by Lodato et al. (2009), the actual energy distribution depends on the stellar structure and only approaches a constant value in the limit of a completely incompressible star. If the star is compressible, the net effect is a more gentle approach to the peak, with significant emission starting at times slightly earlier than t_{min} . The peak fallback rate is consequently decreased with respect to the prediction of equation (6). For example, if the star is modelled as a polytropic sphere of index $\gamma = 1.4$, the peak accretion rate for a black hole mass $M = 10^6 M_{\odot}$ is only $\dot{M}_{\text{p}} \approx 40\dot{M}_{\text{Edd}}$, to be compared with $\dot{M}_{\text{p}} \gtrsim 100\dot{M}_{\text{Edd}}$ for the case of a pure power-law decline. We thus expect that such a more detailed modelling of the fallback rate would result in a suppression of the wind contribution.

We computed the total light curves in several monochromatic bands for the two extreme cases of an incompressible star (pure power-law decline in \dot{M}_{fb}) and for the most compressible star considered by Lodato et al. (2009), with $\gamma = 1.4$. In particular, we computed the fallback rate based on their equations (6)–(9), including the homologous expansion by a factor of ≈ 2.5 , as observed in their numerical simulations.

Fig. 3 shows the total light curves (solid lines), and the separate disc (long-dashed lines) and wind (short-dashed lines) components

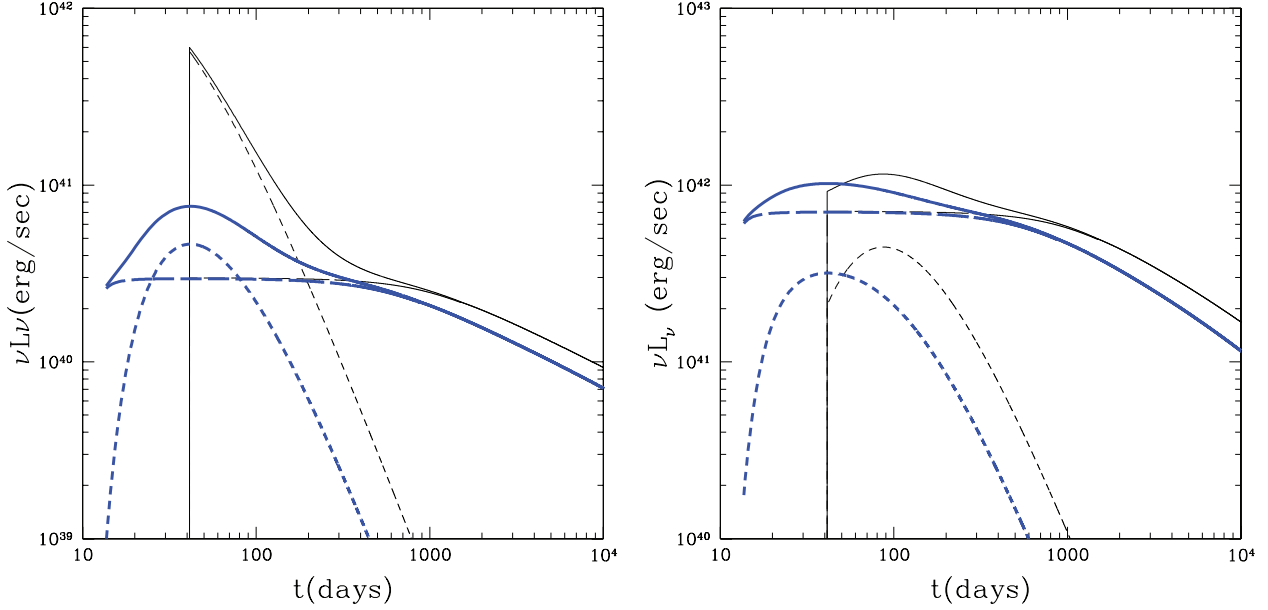


Figure 3. *G*-band (left-hand panel) and FUV (right-hand panel) light curves of tidal disruption events, for a solar-type star, $\beta = 1$, a black hole mass $M = 10^6 M_\odot$, $f_{\text{out}} = 0.1$ and $f_v = 1$. The black curves refer to a pure power-law decline of the fallback rate, while the blue lines adopt the detailed modelling of the stellar structure of Lodato et al. (2009), for $\gamma = 1.4$. The solid lines are the total light curves, the short-dashed line indicates the wind component and the long-dashed line indicates the disc component. In all cases, after ≈ 1 yr, the disc dominates the emission. When a more detailed model for the fallback rate is used, which takes into account the internal structure of the disrupted star, the wind contribution is severely suppressed and only provides a modest contribution in the optical. Light curves for the case of 10^5 - and 10^7 - M_\odot black holes are shown in Figs 4 and 5, respectively.

for $M = 10^6 M_\odot$. We also adopt $f_{\text{out}} = 0.1$ and $f_v = 1$ for the wind (cf. Strubbe & Quataert 2009). The left-hand panel shows the *g*-band light curve, while the right-hand panel shows the FUV one. The black lines correspond to a pure power-law decline in the fallback rate, while the blue lines refer to the Lodato et al. (2009) model. In all cases, after ≈ 1 yr, the disc dominates the emission in all bands and the total light curve follows the $t^{-5/12}$ decline discussed in Section 3. In the FUV band, the disc contribution dominates at all times. In the *g* band, instead, the wind produces a luminous flare, when the fallback rate is modelled as a pure power law. Note that our predicted light curve is slightly different from the one presented in Strubbe & Quataert (2009) (their fig. 3, middle panel). This is because they assume a wider distribution of specific energies (by a factor of 3) and because they have artificially softened the sharp rise to the peak at $t = t_{\text{min}}$ predicted in this case (Strubbe, private communication). At late times, the wind emission declines steeply with time as $t^{-95/36}$, as predicted by the simple scalings of Section 3.

As expected, the effect of a more gentle approach to the peak fallback rate is to severely suppress the wind contribution, which, for a polytropic star of index $\gamma = 1.4$, provides only a modest enhancement of the luminosity in the optical, while the disc emission dominates at almost all times.

We have also computed the same light curves for a smaller black hole, with a mass of $10^5 M_\odot$, and keeping all the other parameters fixed. The results are shown in Fig. 4. For such a smaller black hole, the fallback rate is more strongly super-Eddington and thus the wind contribution is more prominent, even when we adopt the Lodato et al. (2009) model. In this case, the wind light curve in the pure power-law model also shows an initial rise to the peak, before gradually declining as $t^{-95/36}$. This is because T_{obs} initially lies in the Wien part of the blackbody spectrum of the wind photosphere. As the wind photosphere retreats and gets hotter, the observed frequency crosses the blackbody peak and moves to the

Rayleigh–Jeans side, thus producing the peak in the monochromatic light curve (see Section 3).

Finally, we computed the light curves for a more massive black hole, with $M = 10^7 M_\odot$. In this case, the peak fallback rate is only marginally super-Eddington. Even adopting a pure power-law decline, we find that the wind provides a small contribution in the optical (cf. Strubbe & Quataert 2009). With the Lodato et al. (2009) model, the peak fallback rate is $\dot{M}_p \approx 1.3 \dot{M}_{\text{Edd}}$. The wind is thus further suppressed and it produces a negligible contribution at all wavelengths and at all times. The *g*-band, FUV and X-ray light curves are shown in Fig. 5. Even if here the disc dominates at all times, the light curve is not proportional to $t^{-5/3}$ (the red line in the figure) in any single band. Indeed, while in the optical and in the FUV, the light curve follows $t^{-5/12}$, in the X-rays, it initially grows, following the growth of \dot{M} , and then it drops as $t^{-5/3}$ for a short period of time, before eventually declining exponentially.

We thus see that the shape of the wind light curve, which is strongly dependent on the evolution of the fallback rate at early times, is in turn related to the structure of the disrupted star. More incompressible stars give rise to an initially larger fallback rate and are expected to produce a stronger wind contribution.

4.2 Modelling super-Eddington accretion: wind enhancement

The results presented in the previous section are in fact conservative estimates of the wind contribution. Indeed, we have assumed that only 10 per cent of the infalling stellar debris is ejected in the radiatively driven wind, *independently of the fallback rate*. In reality, the strength of the wind is expected to scale with the fallback rate, in such a way that very super-Eddington inflows should result in a much stronger wind. As mentioned above, it is not easy to quantify the fraction f_{out} . We consider here the results of Dotan & Shaviv (2010), who have constructed self-consistent models for

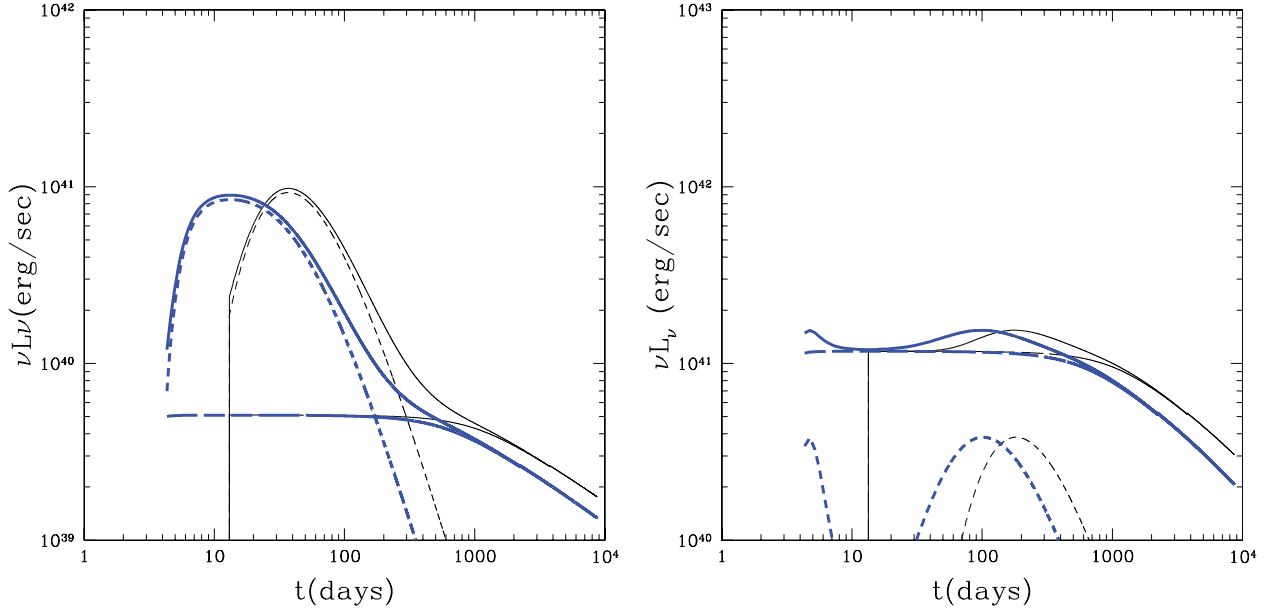


Figure 4. Same as Fig. 3, but for $M = 10^5 M_\odot$.

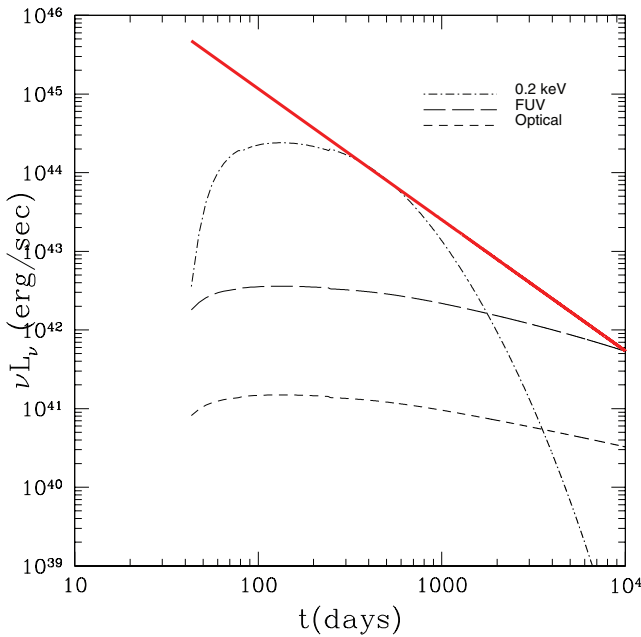


Figure 5. *G*-band (short-dashed line), FUV (long-dashed line) and X-ray in the 0.2-keV band (dot-dashed line) light curves, for $f_{\text{out}} = 0.1$, $f_\nu = 1$, a black hole mass of $10^7 M_\odot$ and our standard parameters $x_* = m_* = \beta = 1$. The red line marks a $t^{-5/3}$ decline.

super-Eddington slim discs. These authors found that the fraction f_{out} is a growing function of the ratio $\dot{M}_{\text{fb}}/\dot{M}_{\text{Edd}}$, reaching values of the order of $f_{\text{out}} \approx 0.7$ for $\dot{M}_{\text{fb}}/\dot{M}_{\text{Edd}} = 20$. For larger values of the infall rate, they did not find any steady-state solution, and it is thus not easy to extrapolate their results beyond that point. We note, however, that when the fallback rate is modelled based on the Lodato et al. (2009) results, the peak rate is not much larger than $20\dot{M}_{\text{Edd}}$ and does not require an extrapolation much beyond their maximum value.

Dotan & Shaviv (2010) constructed four different models of super-Eddington slim discs, with $\dot{M}_{\text{fb}}/\dot{M}_{\text{Edd}} = 1, 5, 10$ and 20 . We have approximated these results using the following relation between f_{out} and $\dot{M}_{\text{fb}}/\dot{M}_{\text{Edd}}$:

$$f_{\text{out}} = \frac{2}{\pi} \arctan \left[\frac{1}{7.5} \left(\frac{\dot{M}_{\text{fb}}}{\dot{M}_{\text{Edd}}} - 1 \right) \right], \quad (28)$$

which has the required properties of approaching zero when $\dot{M}_{\text{fb}} = \dot{M}_{\text{Edd}}$ and of approaching unity when $\dot{M}_{\text{fb}} \gg \dot{M}_{\text{Edd}}$. A comparison between the relation predicted by equation (28) and the Dotan & Shaviv (2010) results is shown in Fig. 6. We have experimented with several different functional relations between f_{out} and $\dot{M}_{\text{fb}}/\dot{M}_{\text{Edd}}$ and found that, as long as the relation reasonably follows the Dotan & Shaviv (2010) data, our resulting light curves are essentially unchanged.

Fig. 7 shows the monochromatic light curves obtained assuming the Lodato et al. (2009) fallback rate for a $\gamma = 1.4$ polytropic star, for $M = 10^6 M_\odot$ (left-hand panel) and $M = 10^5 M_\odot$ (right-hand panel). Clearly, the wind contribution is strongly enhanced and now stands out at early times both in the optical and in the FUV for both choices of the black hole mass. On the other hand, in the X-rays, the disc contribution dominates at all times. After 1–3 yr (depending on the black hole mass), the fallback rate drops to sub-Eddington values and the optical and FUV light curves approach the predicted $t^{-5/12}$ decline, while the X-rays decline exponentially. During the super-Eddington phase, the shape of the light curve depends on the combination of various factors: the time-dependence of both \dot{M}_{fb} and f_{out} , the spectral changes occurring as the wind temperature increases, and the varying relative contribution of the disc and of the wind to the total emission. *Coincidentally*, the FUV light curve for a $10^6 M_\odot$ black hole does initially show a $t^{-5/3}$ decline (shown with a red line in Fig. 6) before flattening into $t^{-5/12}$.

Finally, we considered the case of a more massive black hole, with $10^7 M_\odot$. In this case, the fallback rate is never much larger than the Eddington rate, and thus even when using equation (28) for f_{out} , there is no strong wind, and the emission is at all times completely dominated by the disc.

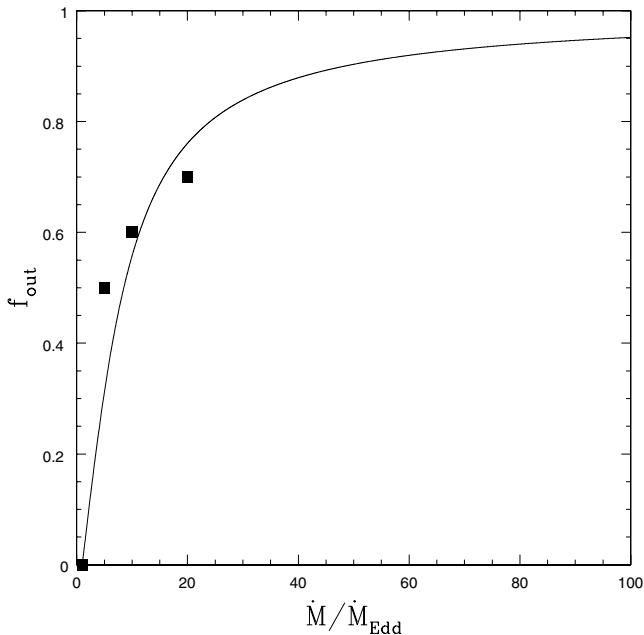


Figure 6. The solid line shows the relation between f_{out} and $\dot{M}_{\text{fb}}/\dot{M}_{\text{Edd}}$ that we have used to model the super-Eddington accretion with a time-dependent fraction of ejected material (equation 28). The squares indicate the results of Dotan & Shaviv (2010).

5 CONCLUSIONS

The ‘signature’ of a tidal disruption event is traditionally considered to be a characteristic evolution of the *fallback rate*, which should follow approximately a $t^{-5/3}$ decline. Indeed, in most cases, candidate tidal disruption events are identified by observing a $t^{-5/3}$

decay in the *luminosity* over the course of a few months at various wavelengths, from the UV (Gezari et al. 2008, 2009) to the X-rays (Esquej et al. 2008; Cappelluti et al. 2009). In this paper, we have critically reviewed the assumptions: (i) that the fallback/accretion rate should follow at all times a $t^{-5/3}$ decay; and (ii) that its behaviour directly translates into the observed light curve decay.

As to the former, the fallback rate behaviour is expected to depend on the star’s internal structure (Lodato et al. 2009). Generally, it displays initially a gentle rise to the peak and approaches a $t^{-5/3}$ decay only several months after the event. In this early stages, the rate is super-Eddington for a black hole of $M < 10^7 M_{\odot}$, and the fraction of mass that accretes on to the hole or is lost in a radiatively driven wind is also time-dependent (Dotan & Shaviv 2010). Under these conditions, the optical and UV light curves may display an initial bump given by the wind emission, which decay rapidly as $t^{-95/36}$. For more massive black holes, the wind is suppressed, since all or nearly all the fallback mass can be accreted, and the light curve at all frequencies is dominated by the disc emission. The detailed evolution and the strength of the wind emission is strongly dependent on the evolution of the fallback rate at early times, and is thus very sensitive to the internal structure of the disrupted star (Lodato et al. 2009).

Likewise, at higher frequencies and at later times, the wind emission is negligible for all black hole masses. Also in this cases, while the bolometric curve may decline as $t^{-5/3}$, the monochromatic light curves in general do not. On a time-scale of months to years, the optical and UV light curves are expected to decrease much slower, as $t^{-5/12}$. Only in X-rays does the light curve initially follow more closely the bolometric luminosity, hence showing an approximately $t^{-5/3}$ decline, before steepening into an exponential drop after a few years. The predicted X-ray luminosities in the first year after the disruption are comparable to those of bright quasars. Detectability

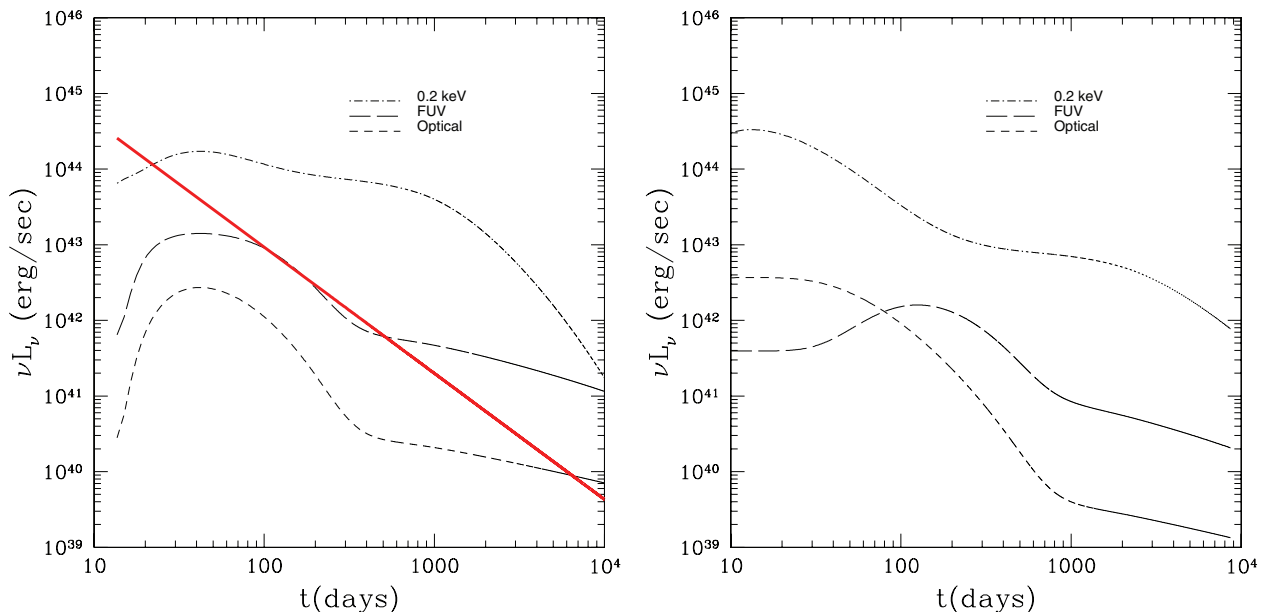


Figure 7. Optical (*G*-band, short-dashed lines), FUV (in the GALEX FUV band, long-dashed lines) and X-ray (at 0.2 keV, dot-dashed lines) light curves obtained by adopting a time-dependent model for f_{out} (equation 28), for $M = 10^6 M_{\odot}$ (left-hand panel) and $M = 10^5 M_{\odot}$ (right-hand panel). We also assume the Lodato et al. (2009) fallback rate for a $\gamma = 1.4$ polytropic star. The other parameters are $x_* = m_* = \beta = 1$. The red line in the left-hand panel shows, for comparison, a $t^{-5/3}$ decline. In this case, the wind contribution is strongly enhanced and now stands out both in the optical and in the FUV. On the contrary, the X-ray light curve is at all times dominated by the disc. The slight ‘bends’ in the X-ray light curves are a consequence of the fact that, during the super-Eddington phase, only a (time-dependent) fraction of the fallback material makes it to the hole.

is thus not an issue in the local Universe, and a standard snapshot survey with currently flying detectors would give enough accuracy to constrain the slope with two epochs of observation. Coincidentally, for some combinations of the model parameters, the FUV light curve might exhibit a decline seemingly close to $t^{-5/3}$, although clearly this does not reflect the time-evolution of the fallback rate.

Typically, observed tidal disruption event candidates have UV/optical luminosities in excess of 10^{43} erg s⁻¹ and light curves, which decrease more steeply than $t^{-5/12}$. This indicates that even in the FUV the wind contribution might dominate at early times, consistent with our models which adopt a time-dependent ejected mass fraction (see e.g. Fig. 7, left-hand panel). We conclude that a more sophisticated – ideally multiwavelength – modelling of the data than done so far is required to pin down a tidal disruption event and derive the system parameters. The X-ray band seems best suited to identify a tidal disruption event through the fallback decay rate, while early optical and UV observations can catch at early times the wind emission, which would also teach us about the ill-known super-Eddington accretion physics and possibly even about the structure of the disrupted star.

ACKNOWLEDGMENTS

We would like to thank Linda Strubbe and Eliot Quataert for stimulating discussions about their work. GL acknowledges the hospitality of the Racah Institute of Physics in Jerusalem, where a large part of this work was done.

REFERENCES

- Ayal S., Livio M., Piran T., 2000, *ApJ*, 545, 772
 Blandford R. D., Begelman M. C., 2004, *MNRAS*, 349, 68
 Cannizzo J. K., Lee H. M., Goodman J., 1990, *ApJ*, 351, 38
 Cappelluti N. et al., 2009, *A&A*, 495, L9
 Dotan C., Shaviv N. J., 2010, preprint (arXiv:1004.1797)
 Esquej P. et al., 2008, *A&A*, 489, 543
 Evans C. R., Kochanek C. S., 1989, *ApJ*, 346, L13
 Gezari S. et al., 2008, *ApJ*, 676, 944
 Gezari S. et al., 2009, *ApJ*, 698, 1367
 Kasen D., Ramirez-Ruiz E., 2010, *ApJ*, 714, 155
 Komossa S., Bade N., 1999, *A&A*, 343, 775
 Lacy J. H., Townes C. H., Hollenbach D. J., 1982, *ApJ*, 262, 120
 Laguna P., Miller W. A., Zurek W. H., Davies M. B., 1993, *ApJ*, 410, L83
 Lodato G., King A. R., Pringle J. E., 2009, *MNRAS*, 392, 332
 Magorrian J., Tremaine S., 1999, *MNRAS*, 309, 447
 Nolthenius R. A., Katz J. I., 1982, *ApJ*, 263, 377
 Phinney E. S., 1989, in Morris M., ed., *IAU Symp. Vol. 136, Manifestations of a Massive Black Hole in the Galactic Center*. Kluwer, Dordrecht, p. 543
 Rees M. J., 1988, *Nat*, 333, 523
 Rossi E. M., Begelman M. C., 2009, *MNRAS*, 392, 1451
 Rosswog S., 2007, *MNRAS*, 376, L48
 Rosswog S., Ramirez-Ruiz E., Hix W. R., 2008, *ApJ*, 679, 1385
 Sigurdsson S., Rees M. J., 1997, *MNRAS*, 284, 318
 Strubbe L. E., Quataert E., 2009, *MNRAS*, 400, 2070
 Syer D., Ulmer A., 1999, *MNRAS*, 306, 35
 Ulmer A., 1999, *ApJ*, 514, 180

This paper has been typeset from a $\text{\TeX}/\text{\LaTeX}$ file prepared by the author.